NACA RM E53B03

9089

NACA

RESEARCH MEMORANDUM

AERODYNAMICS OF SLENDER BODIES AT MACH NUMBER OF 3.12 AND

REYNOLDS NUMBERS FROM 2×10^6 TO 15×10^6

III - BOUNDARY LAYER AND FORCE MEASUREMENTS ON A

SLENDER CONE-CYLINDER BODY OF REVOLUTION

By John R. Jack

Lewis Flight Propulsion Laboratory
Cleveland, Ohio

Classification cancelled (or changed to ...UNCLASSIFIED......)

By Authority of ...NASA.. Tech Pub Announcement #2......
                    (OFFICER AUTHORIZED TO CHANGE)

By.................................... 16 Dec 58 ....
      I.... AND

              ...(MMB)...............................
    GRADE OF OFFICER MAKING CHANGE)

...31 May 61... CLASSIFIED DOCUMENT

NATIONAL ADVISORY COMMITTEE
FOR AERONAUTICS
WASHINGTON
April 6, 1953

NATIONAL ADVISORY COMMITTEE FOR AERONAUTICS

RESEARCH MEMORANDUM

AERODYNAMICS OF SLENDER BODIES AT MACH NUMBER OF 3.12 AND

REYNOLDS NUMBERS FROM 2×10^6 TO 15×10^6

III - BOUNDARY LAYER AND FORCE MEASUREMENTS ON A

SLENDER CONE-CYLINDER BODY OF REVOLUTION

By John R. Jack

SUMMARY

An experimental investigation to determine the aerodynamic charac-
teristics of a slender cone-cylinder body of revolution was conducted
in the NACA Lewis 1- by 1-foot supersonic wind tunnel. Viscous drag and
three component forces were measured at a Mach number of 3.12 for a Rey-
nolds number range from 2×10^6 to 14×10^6 (based on model length) and for
an angle-of-attack range from zero to 9°.

For zero angle of attack, the total-drag coefficient increased with
increasing Reynolds number until a Reynolds number of approximately
5.0×10^6 was reached and then remained practically unchanged. A break-
down into components of the total measured drag for a Reynolds number of
14×10^6 and for angle of attack showed that the increment in skin-friction
coefficient due to angle of attack was small compared with that of the
total-drag coefficient. Theoretical values of the fore-pressure drag,
lift, and pitching-moment coefficients obtained from combining a second-
order axial-flow solution with a first-order cross-flow solution were
calculated for comparison with the experimental results.

INTRODUCTION

As part of a systematic program to ascertain the effects of Reynolds
number on aerodynamic characteristics, to extend the basic information
on the aerodynamics of bodies of revolution, and to assess the validity
of several theories for predicting pressures and forces acting on bodies,
tests are being conducted in the NACA Lewis 1- by 1-foot supersonic wind
tunnel on a series of bodies of revolution. The first of this series of
investigations is reported in reference 1, which contains an appraisal

of the aerodynamics of a near-parabolic nose body. The results of the
second investigation are reported in reference 2, which is concerned with
the aerodynamic load distributions of a series of five bodies having
conical or slightly blunted noses and cylindrical afterbodies. The sub-
ject of the present report is the boundary-layer development and forces
acting on a typical cone-cylinder body of revolution at a Mach number
of 3.12.

The boundary-layer development on the model and the forces acting
on the model were determined for a range of Reynolds numbers from 2×10^6
to 14×10^6 (based on body length) and angles of attack from zero to $9°$.
These data are compared with the compressible boundary-layer theory for
cones and with the hybrid theory of reference 3 for the forces.

SYMBOLS

The following symbols are used in this report:

A_F frontal area

C_D drag coefficient, $D/q_0 A_F$

C_L lift coefficient, $L/q_0 A_F$

C_M pitching-moment coefficient about base of model, $m_p/q_0 A_F l$

C_p pressure coefficient, $(p-p_0)/q_0$

D drag

d maximum body diameter

L lift force

l body length

M Mach number

m_p pitching moment

p static pressure

q dynamic pressure, $(\gamma/2)pM^2$

Re Reynolds number, $\rho U l/\mu$

Re_x Reynolds number based on length x

2738

U   free-stream velocity

u   velocity in boundary layer

x, r, θ cylindrical coordinates

α angle of attack

γ ratio of specific heats, 1.40

δ^* displacement thickness, $\dfrac{1}{\rho_1 u_1} \displaystyle\int_0^\infty (\rho_1 u_1 - \rho u)\,dy$

θ momentum thickness, $\dfrac{1}{\rho_1 u_1^2} \displaystyle\int_0^\infty \rho u (u_1 - u)\,dy$

μ viscosity

ρ density

Subscripts:

0   free-stream conditions

1   conditions at edge of boundary layer

b   base

f   friction

p   pressure

APPARATUS AND PROCEDURE

The investigation was conducted in the Lewis 1- by 1-foot variable Reynolds number tunnel, which is a continuous-flow, nonreturn-type tunnel having a test section Mach number of 3.12 ±0.03. Inlet pressures were varied from 7 to 50 pounds per square inch absolute, and a stagnation temperature of approximately 60° F was maintained throughout the investigation. The entering air had a specific humidity of approximately 2×10^{-5} pounds of water per pound of dry air, which insured negligible condensation effects.

A schematic diagram with the pertinent dimensions of the pressure-distribution model used to obtain the boundary-layer data is given in figure 1. This model has a nose fineness ratio (l/d) of 6 and an over-all fineness ratio of 12. The boundary-layer data for zero angle of attack were obtained by probing the side $(\theta = 90^\circ)$ of the body at six axial stations $(x = 4, 7, 11.8, 14, 17,$ and 21 in.) with the probe illustrated in figure 2. The force model was the same as the pressure-distribution model except that it was fabricated from aluminum instead of steel. A three-component strain-gage balance, which was attached to a sting-strut combination, supported the force model. Since the strain gage was mounted internally, no aerodynamic tare corrections were necessary. The maximum experimental errors in the force coefficients are believed to be as follows for the lowest and highest Reynolds numbers, respectively:

Force coefficient	Maximum probable error at Reynolds number, Re	
	2×10^6	14×10^6
c_D	±0.01	±0.002
c_L	$\pm.02$	$\pm.002$
c_M	$\pm.002$	$\pm.001$

Both the pressure-distribution model and the force model were supported from their bases by a sting extending upstream from a horizontal strut mounted to the side wall of the tunnel (fig. 1). In order to obtain minimum interference with the base pressures at zero angle of attack, the sting was designed with the aid of the data presented in reference 4. The model was rotated about a point 4 inches upstream of its base for angle of attack.

REDUCTION OF DATA AND METHODS OF COMPUTATION

The boundary-layer-survey data were evaluated by the Rankine-Hugoniot equation with the assumption that the total temperature was constant in the flow field and that the static pressure was constant along lines normal to the body surface. With these assumptions, velocity profiles were calculated from the known Mach number profiles with the use of the following identity:

$$\frac{u}{u_1} = \frac{M}{M_1}\sqrt{\frac{1 + \frac{\gamma-1}{2} M_1^2}{1 + \frac{\gamma-1}{2} M^2}} \tag{1}$$

2773

From the velocity profiles at the various axial stations, the boundary-layer-displacement and momentum thicknesses may be obtained from

$$\delta^* = \int_0^\infty \left(1 - \frac{\rho}{\rho_1}\frac{u}{u_1}\right) dy \tag{2}$$

$$\theta = \int_0^\infty \frac{\rho}{\rho_1} \left(\frac{u}{u_1} - \frac{u^2}{u_1^2}\right) dy \tag{3}$$

where $\frac{\rho}{\rho_1} = \dfrac{1 + \frac{\gamma-1}{2} M^2}{1 + \frac{\gamma-1}{2} M_1^2}$ and y is measured normal to the body surface.

With the displacement and momentum thicknesses known, the mean skin-friction-drag coefficients were then calculated by using the following equation:

$$C_{D,f} = \frac{2\pi}{q_0 A_F}\left[\int_0^s \frac{d(r\rho_1 u_1^2 \theta)}{ds} ds - \int_0^s r\delta^* \frac{dp}{ds} ds\right] \tag{4}$$

where s represents the distance measured along the body surface. Equation (4) may be derived from the boundary-layer momentum equation for axially symmetric flow with the assumption that the boundary-layer thickness δ is very much less than the body radius (see, for example, ref. 5, pp. 19 and 20). The second term of equation (4) may be neglected since it has been shown that the contribution of the pressure-gradient term to $C_{D,f}$ is very small (see ref. 6).

Theoretical force coefficients for the body at angle of attack were calculated by first obtaining the pressure distributions for the body by the hybrid theory of reference 3 and integrating these numerically to obtain the forces. The hybrid theory of reference 3 is founded on the assumption that the first-order theory of reference 7 yields an adequate cross-flow solution because of the smaller disturbances involved, but a second-order or more exact solution is needed for the axial flow. With the two solutions combined and with the exact isentropic pressure relation used, the pressure coefficient at any point is

$$C_p = \frac{2}{\gamma M_0^2}\left\{\left[1 + \frac{\gamma-1}{2} M_0^2 \left(1 - \frac{q^2}{U^2}\right)\right]^{\frac{\gamma}{\gamma-1}} - 1\right\} \tag{5}$$

where

$$\left(\frac{q}{U}\right)^2 = \left(\frac{v_x}{U}\right)^2 + \left(\frac{v_r}{U}\right)^2 + \left(\frac{v_\theta}{U}\right)^2$$

$$\frac{v_x}{U} = \cos\alpha - \varphi_{1,x}\sin\alpha\cos\theta + \varphi_{2,x}\cos\alpha$$

$$\frac{v_r}{U} = -\sin\alpha\cos\theta - \varphi_{1,r}\sin\alpha\cos\theta + \varphi_{2,r}\cos\alpha$$

$$\frac{v_\theta}{U} = \sin\alpha\sin\theta + \varphi_{1,\theta}/r\ \sin\alpha\sin\theta$$

φ_1 = first-order perturbation potential for cross flow

φ_2 = second-order perturbation potential for axial flow

First-order cross-flow terms were calculated by the method of reference 7 and second-order terms were obtained by the method of reference 3. Theoretical force coefficients for the body at angle of attack were also calculated by adding the viscous cross-flow effect to the hybrid theory of reference 3 (see, for example, ref. 3).

RESULTS AND DISCUSSION

Pressure Distributions

For completeness, the pressure distribution at zero angle of attack for Reynolds numbers of 2×10^6, 8×10^6, and 14×10^6 obtained from reference 2 are presented in figure 3.[1] Also given in figure 3 are the theoretical curves computed from the second-order theory of reference 3. Agreement between experiment and the second-order theory is very good for the Reynolds number range investigated. Figure 4 shows the variation of base-pressure coefficient with angle of attack for three Reynolds numbers. Detailed pressure-distribution results for this cone-cylinder model at angle of attack and for a range of Reynolds numbers from 2×10^6 to 14×10^6 may be found in reference 2.

---

[1]Because of diffusion of atmospheric air through the flexible plastic tubing used in the manometer system (see ref. 2), pressure distributions presented in reference 2 for the lowest Reynolds number of 2×10^6 were slightly in error. The measurements presented herein were repeated with new model instrumentation and with the diffusion of air into the manometer system practically eliminated.

Boundary Layer

For an experimental correlation of the component drag forces which make up the total drag of the model at zero angle of attack, the movement of transition and total friction-drag coefficients were determined for a range of Reynolds numbers.

The movement of transition was determined with the aid of the schlieren system by taking many microsecond schlieren pictures at the same condition and by averaging the top ($\theta = 180^{\circ}$) and bottom ($\theta = 0^{\circ}$) location of the beginning of transition. Figure 5(a) shows the variation of the beginning of transition with free-stream Reynolds number. This curve is very similar to that presented in reference 1 except that it is displaced slightly towards the tip of the model. Figure 5(b) illustrates the behavior of the transition Reynolds number with inlet pressure. Originally this behavior had been attributed to a change in turbulence level or a change in tunnel wall boundary-layer development; however, recently the Naval Ordnance laboratory has obtained similar data in their Pressurized Ballistics Range (ref. 8). Since the turbulence level is small and there is no tunnel boundary layer in this facility, the change in transition Reynolds number with inlet pressure cannot be attributed solely to either of these factors.

The experimental skin-friction-drag coefficients for the six axial stations probed are presented in figure 6 for the range of Reynolds numbers investigated. A comparison of the experimental skin-friction coefficients with the theoretical coefficients obtained from the two-dimensional boundary-layer theories and with those obtained from the transformation presented in reference 9 is also given in figure 5. The basic two-dimensional boundary-layer theories used to make the calculations were the Chapman and Rubesin theory for laminar flows (ref. 10), the extended Frankl and Voishel theory (ref. 11), and the Van Driest theory for turbulent flows (ref. 12). All the above-mentioned theories as used are for flat plates with zero pressure gradients and zero heat transfer. Mangler's derivation (ref. 8) transforms laminar skin-friction coefficients for two-dimensional bodies to those for bodies of revolution with analogous pressure distributions. Since it is shown in reference 6 that the pressure-gradient contribution to the mean skin-friction coefficient is small, the conical transformation is used for comparison; that is,

$$c_{D,f} = \frac{2}{\sqrt{3}} \, c_{D,f}(\text{flat plate}) \tag{8}$$

The transition data presented in figure 5(a) indicate that the total skin-friction coefficients for the first axial station at each of the free-stream Reynolds numbers investigated should be laminar; yet the three coefficients do not agree with theory. These discrepancies might

The effect of angle of attack on the total-drag coefficient is given in figure 9 for three Reynolds numbers. For the lower angles of attack, the drag coefficient increased with increasing Reynolds number up to a Reynolds number of approximately 8×10^6 and then remained relatively constant. At angles of attack greater than 6°, the drag coefficient increased continuously with Reynolds number for the Reynolds number range investigated.

In evaluating performance characteristics of supersonic missiles, the variation of total drag with angle of attack is quite important and, consequently, the variation of friction drag with angle of attack becomes significant since it can contribute as much as 50 percent to the total drag. Therefore, in order to give an insight into this behavior, the fore-pressure- and base-pressure-drag coefficients for a Reynolds number of 14×10^6 have been subtracted from the total-drag coefficient to give the variation of skin-friction coefficient with angle of attack (fig. 10). This has been done for a Reynolds number of 14×10^6 since the higher Reynolds numbers are of more practical concern. It must be pointed out, however, that the variation of skin-friction coefficient with angle of attack is only qualitative since this calculation involved a numerical integration to obtain the fore-pressure-drag coefficient and, consequently, may be in error. Figure 10 does indicate, however, that the variation of the increment in skin friction due to angle of attack is small compared with the total-drag increment.

Also presented in figure 10(a) is a comparison between the pressure-drag increment due to angle of attack and the theory of reference 3. This comparison shows that the theory of reference 3 is in good agreement with experiment up to an angle of attack of 6°, but from 6° to 9° the theory predicts values much too low. The lack of agreement at the high angles of attack appears to be due to effects not considered in the potential equation, namely, the viscous cross-flow effects. By adding the viscous cross-flow effects as suggested in reference 3 to the potential theory of reference 3, the increment in experimental fore-pressure drag due to angle of attack is predicted closely (fig. 10(b)).

Experimental results showing the variation of lift coefficient with angle of attack are compared with the hybrid theory of reference 3 in figure 11. Agreement between experiment and theory is fair up to a 3° angle of attack, but the predictions of the theory for the higher angles of attack are quite low. Again, adding the viscous effect to the theory of reference 3 brings the theoretical lift variation into fair agreement with experiment.

The experimental variation of the pitching-moment coefficient about the base of the model and the center of pressure are given in figures 12 and 13, respectively. The trends of the experimental pitching moment and center of pressure with angle of attack are predicted by the theory of

reference 3 with the addition of the viscous cross-flow effect. The magnitude of the experimental values of the pitching moment and the center of pressure is, however, higher than would be predicted by theory. As in the case of the lift coefficient, the effect of Reynolds number is small.

SUMMARY OF RESULTS

The aerodynamic characteristics of a slender cone-cylinder body of revolution were investigated in the NACA Lewis 1- by 1-foot variable Reynolds number tunnel at a Mach number of 3.12. The results may be summarized as follows:

1. The total-drag coefficient for zero angle of attack increased with increasing Reynolds number until a Reynolds number of approximately 5.0×10^6 was reached and then remained relatively constant.

2. A breakdown of the total measured drag into components for a Reynolds number of 14×10^6 and for angle of attack showed that the increment in skin-friction-drag coefficient due to angle of attack was small compared with that of the total-drag coefficient.

3. Experimentally measured drag and lift were in good agreement with Van Dykes' hybrid theory at small angles of attack. By adding the viscous cross-flow effect to the hybrid theory, much better agreement between experiment and theory was obtained for all angles of attack.

4. The trends of the experimental pitching moment and center of pressure with angle of attack are predicted by Van Dykes' hybrid theory with the addition of the viscous cross-flow effect; however, the magnitude of the experimental values was higher than the theory would predict.

Lewis Flight Propulsion Laboratory
    National Advisory Committee for Aeronautics
   Cleveland, Ohio

REFERENCES

1. Jack, John R., and Burgess, Warren C.: Aerodynamics of Slender Bodies at Mach Number of 3.12 and Reynolds Numbers from 2×10^6 to 15×10^6. I - Body of Revolution with Near-Parabolic Forebody and Cylindrical Afterbody. NACA RM E51H13, 1951.

2. Jack, John R., and Gould, Lawrence D.: Aerodynamics of Slender
     Bodies at Mach Number of 3.12 and Reynolds Numbers from 2×10^6 to
     15×10^6. II - Aerodynamic Load Distributions of Series of Five
     Bodies Having Conical Noses and Cylindrical Afterbodies.
     NACA RM E52C10, 1952.

3. Van Dyke, Milton D.: First- and Second-Order Theory of Supersonic
     Flow Past Bodies of Revolution. Jour. Aero. Sci., vol. 18, no. 3,
     Mar. 1951, pp. 161-178.

4. Chapman, Dean R.: An Analysis of Base Pressure at Supersonic Veloc-
     ities and Comparison with Experiment. NACA Rep. 1051, 1951.
     (Supersedes NACA TN 2137.)

5. Young, A. D.: Modern Developments in Fluid Dynamics. Vol. III.
     Chap. X. Boundary Layers. The College of Aeronautics, Cranfield,
     1949.

6. Jack, John R.: Aerodynamic Characteristics of a Slender Cone-
     Cylinder Body of Revolution at a Mach Number of 3.85. NACA
     RM E51H17, 1951.

7. Tsien, Hsue-Shen: Supersonic Flow over an Inclined Body of Revolu-
     tion. Jour. Aero. Sci., vol. 5, no. 12, Oct. 1938, pp. 480-483.

8. Potter, J. L.: New Experimental Investigations of Friction Drag and
     Boundary Layer Transition on Bodies of Revolution at Supersonic
     Speeds. Paper presented at Second bur. Ordnance Symposium on
     Aeroballistics, Pasadena (Calif.), May 13-15, 1952.

9. Mangler, W.: Compressible Boundary Layers on Bodies of Revolution.
     VG 83, No. 47T, M.A.P. Volkenrode.

10. Chapman, Dean R., and Rubesin, Morris W.: Temperature and Velocity
     Profiles in the Compressible Laminar Boundary Layer with Arbitrary
     Distribution of Surface Temperature. Jour. Aero. Sci., vol. 16,
     no. 9, Sept. 1949, pp. 547-565.

11. Rubesin, Morris W., Maydew, Randall C., and Vargo, Steven A.: An
     Analytical and Experimental Investigation of the Skin Friction of
     the Turbulent Boundary Layer on a Flat Plate at Supersonic Speeds.
     NACA TN 2305, 1951.

12. Van Driest, E. R.: Turbulent Boundary Layer in Compressible Fluids.
     Jour. Aero. Sci., vol. 18, no. 3, Mar. 1951, pp. 145-161.

13. Blue, Robert E., and Low, George M.: Factors Affecting Laminar
    Boundary Layer Measurements in a Supersonic Stream.
    NACA TN 2891, 1953.

14. Moore, Franklin K.: Use of the Boundary Layer of a Cone to Measure
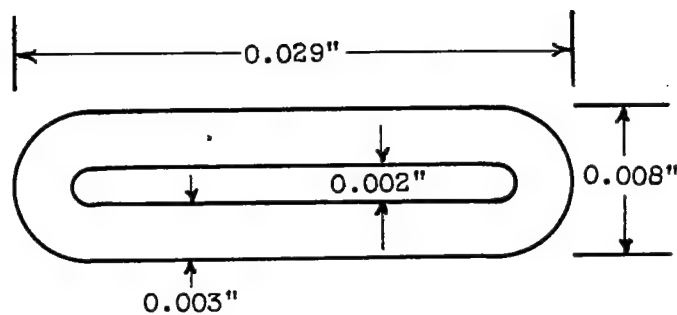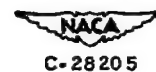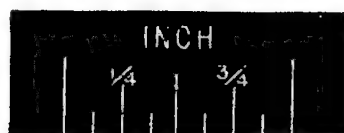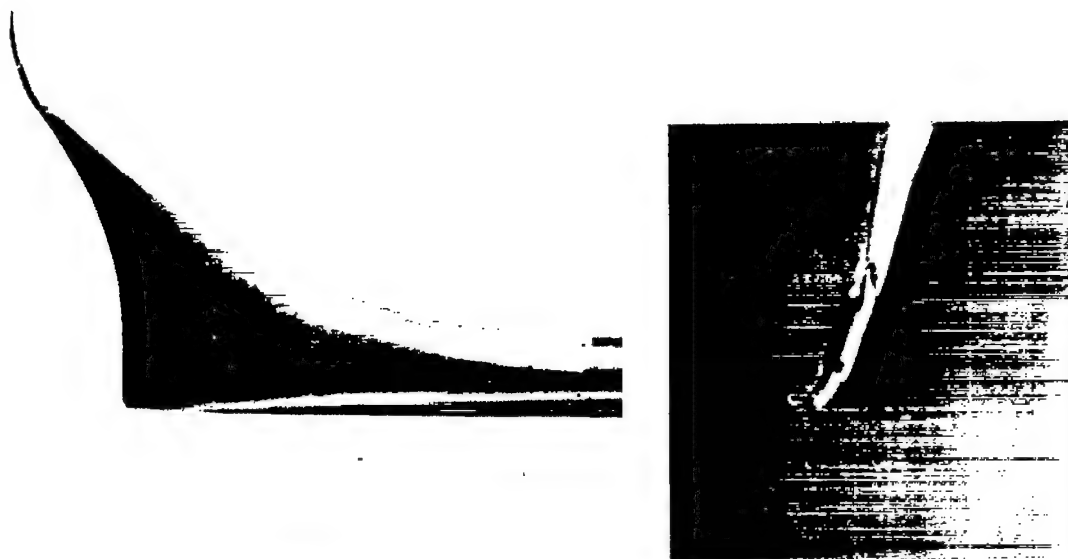   Supersonic Flow Inclination. NACA TN 2723, 1952.

2738
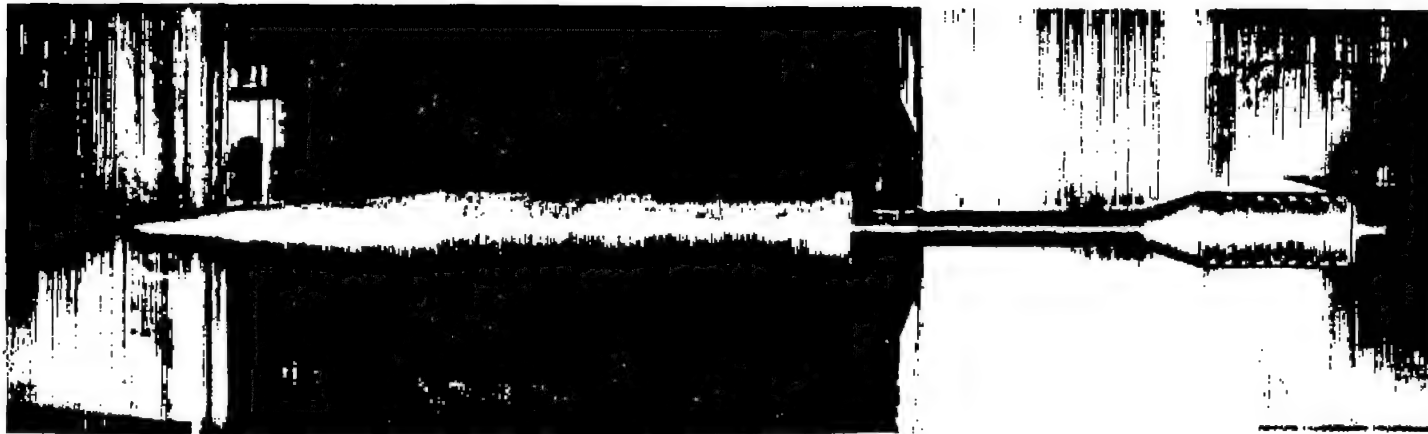
(a) Photograph of model installed in Lewis 1- by 1-foot supersonic wind tunnel.
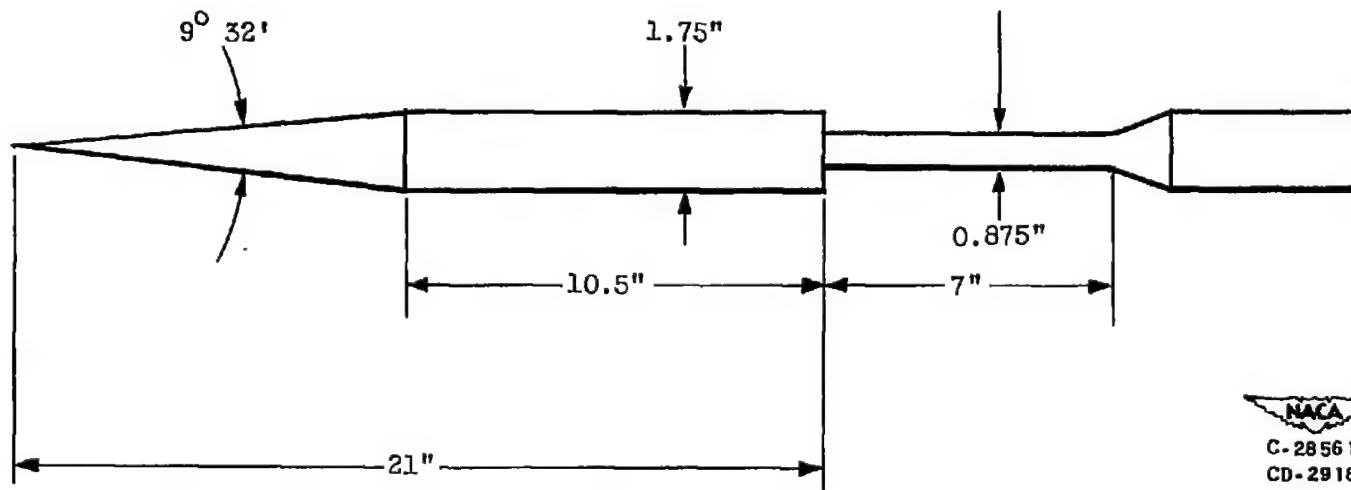
(b) Schematic drawing of model.

Figure 1. - Model used in investigation.

2738

C-28205

Enlarged view of probe opening

Figure 2. - Probe used to obtain boundary-layer data at zero angle of attack.

(a) Reynolds number Re, 2×10^6.

(b) Reynolds number Re, 8×10^6.

(c) Reynolds number Re, 14×10^6.
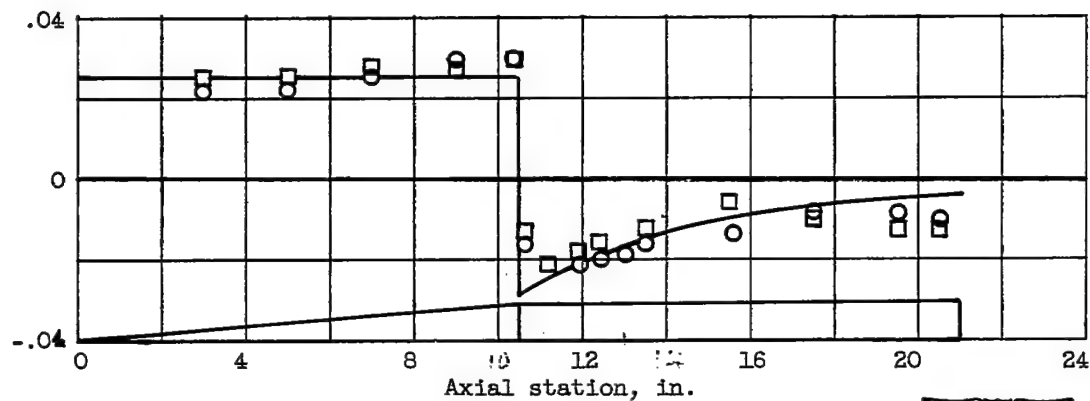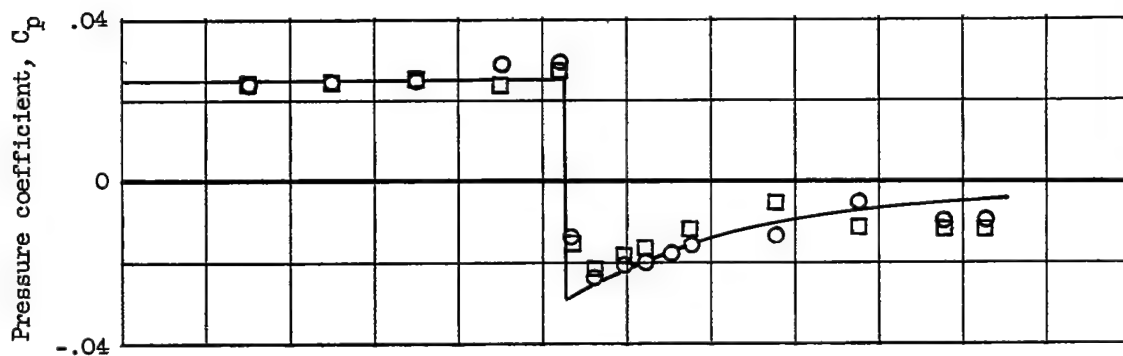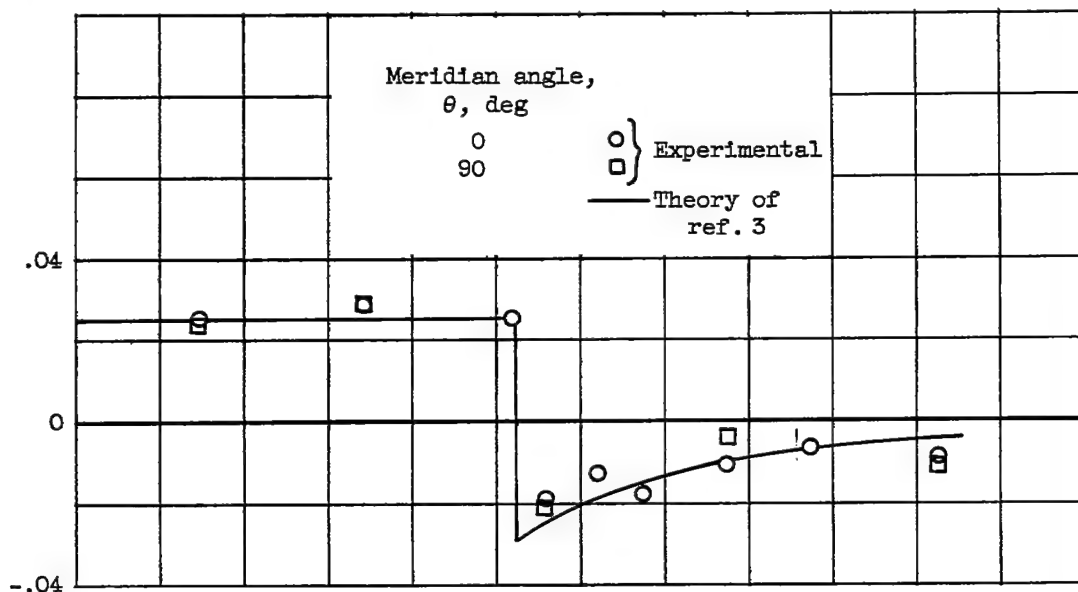
Figure 3. - Experimental and theoretical axial variation of pressure coefficient for model at zero angle of attack.
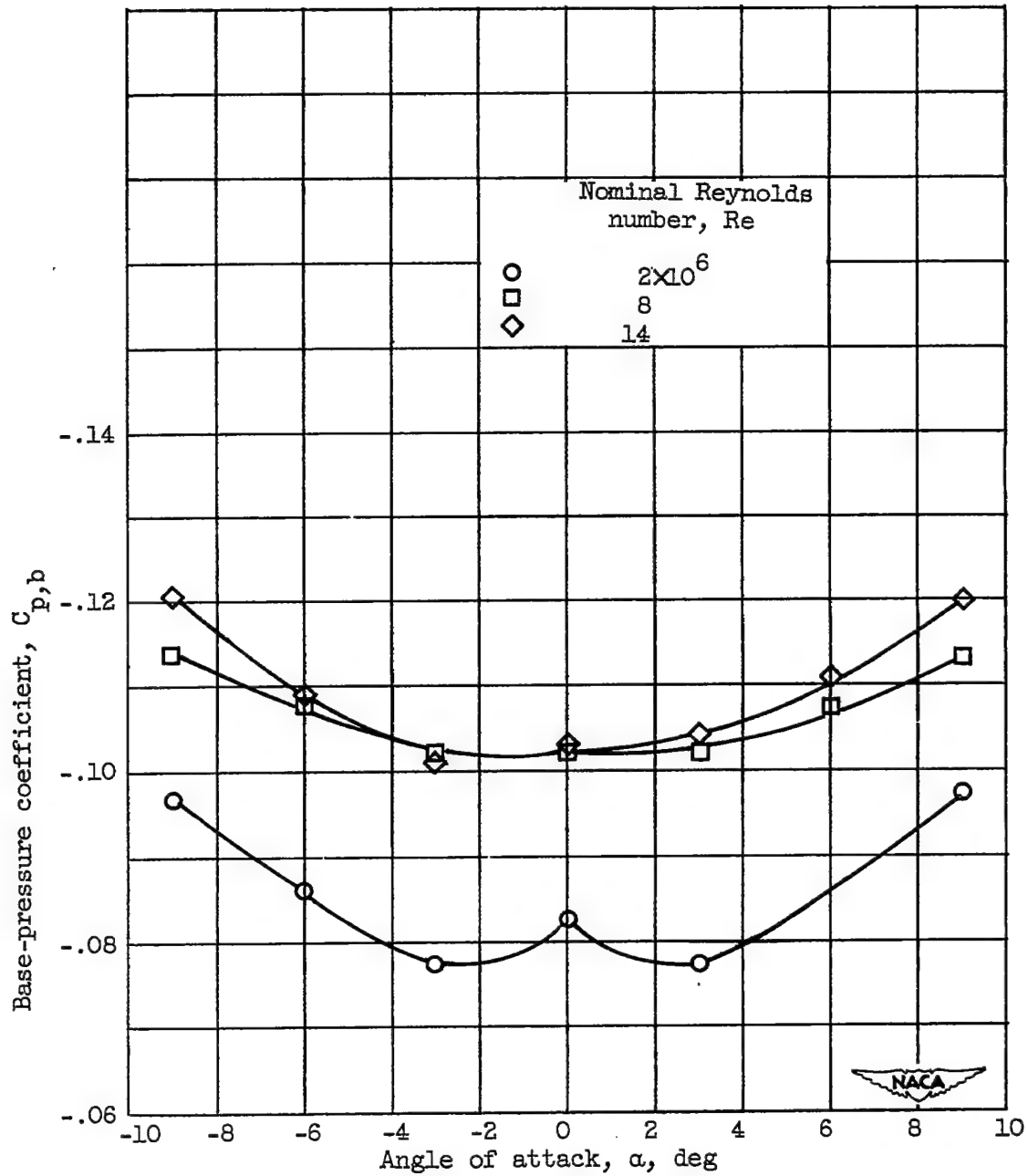
Figure 4. - Variation of base-pressure coefficient with angle of attack for Reynolds numbers of 2×10^6, 8×10^6, and 14×10^6.

2738
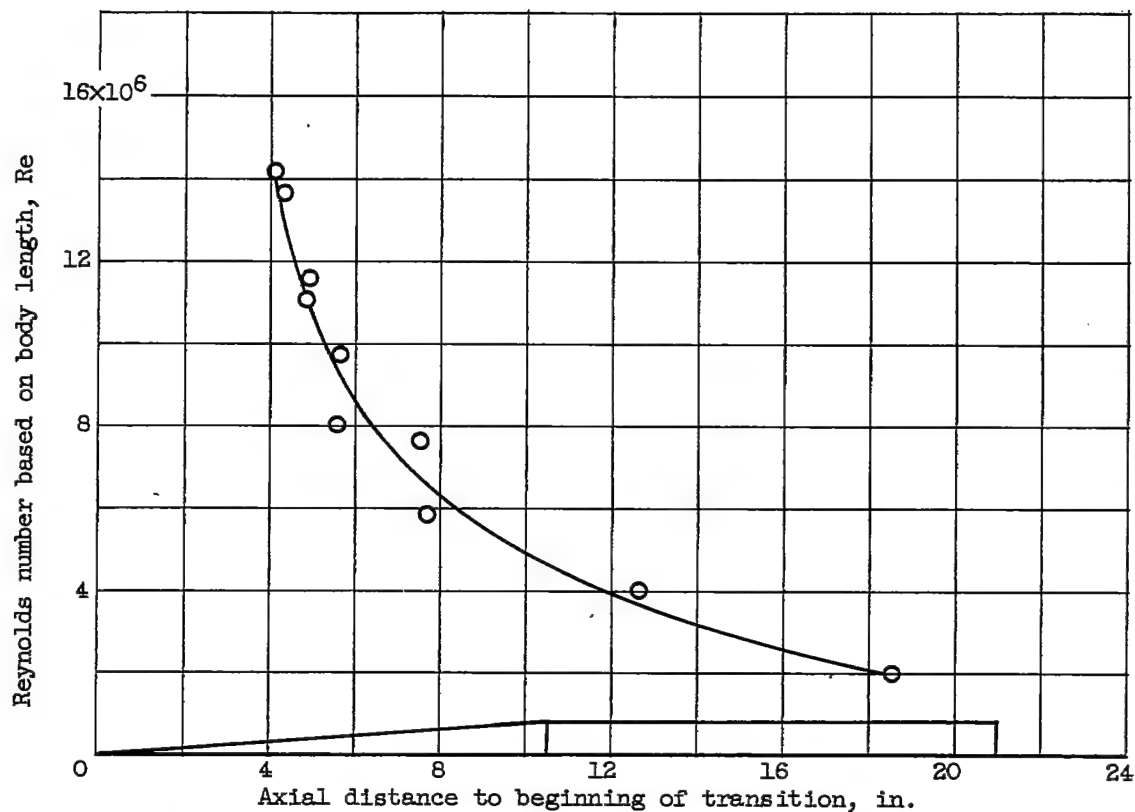
(a) Effect of free-stream Reynolds number upon axial distance to beginning of transition.
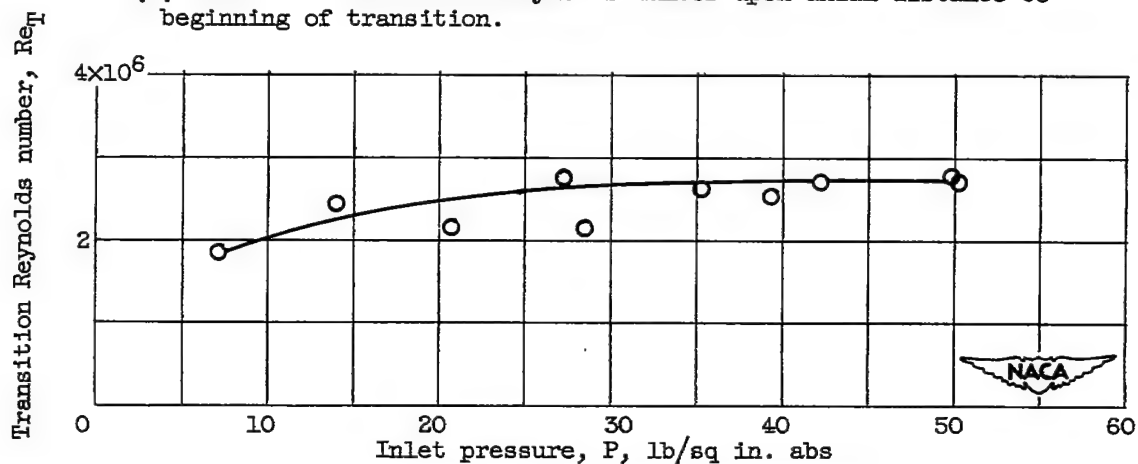
(b) Effect of inlet pressure upon transition Reynolds number.

Figure 5. - Variation of boundary-layer transition with inlet pressure and free-stream Reynolds number.
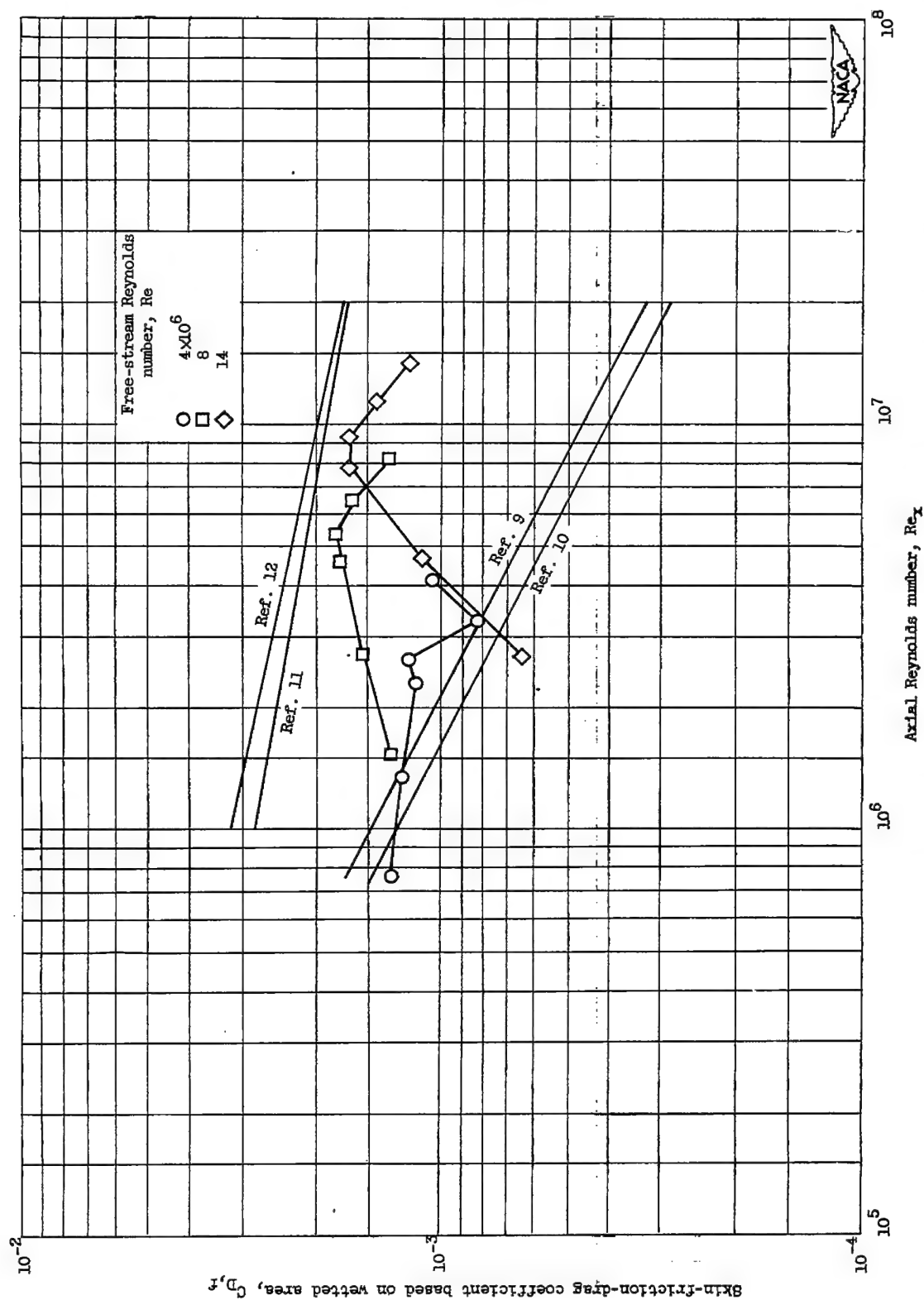
Figure 6. - Variation of total skin-friction coefficient with axial Reynolds number for zero angle of attack.

2738

(a) Variation of displacement thickness with axial station.

(b) Variation of momentum thickness with axial station.
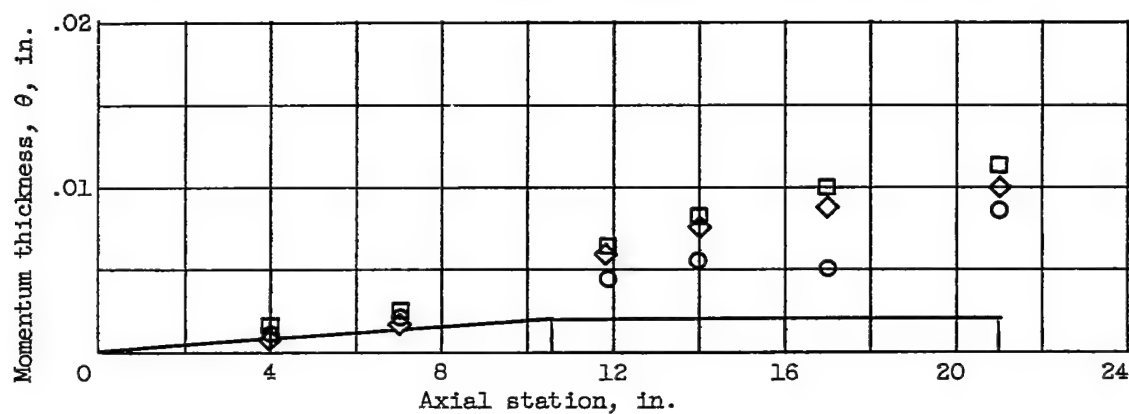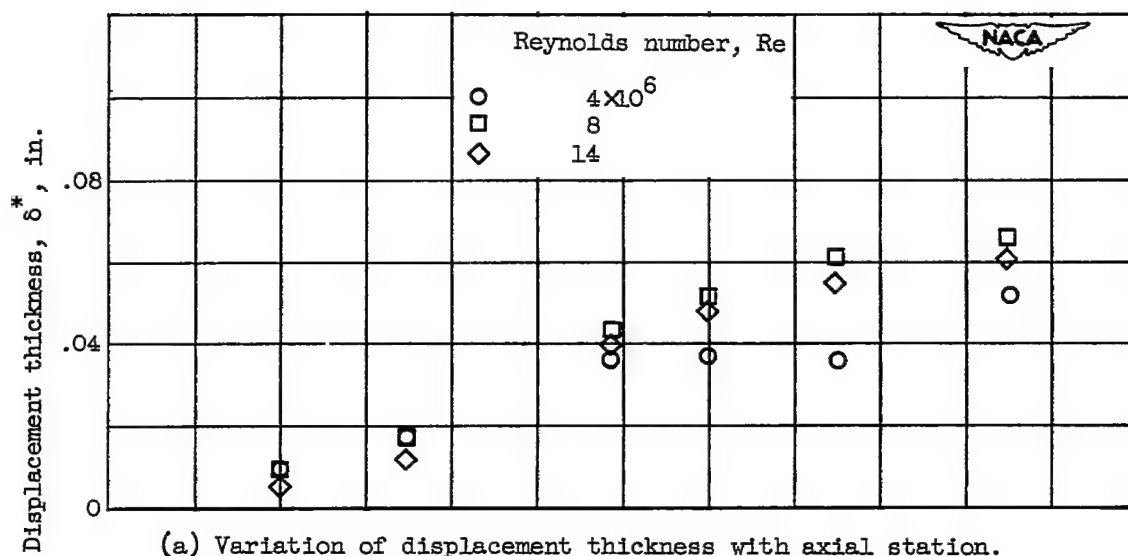
Figure 7. - Displacement- and momentum-thickness distributions on model for Reynolds numbers of 4×10^6, 8×10^6, and 14×10^6.
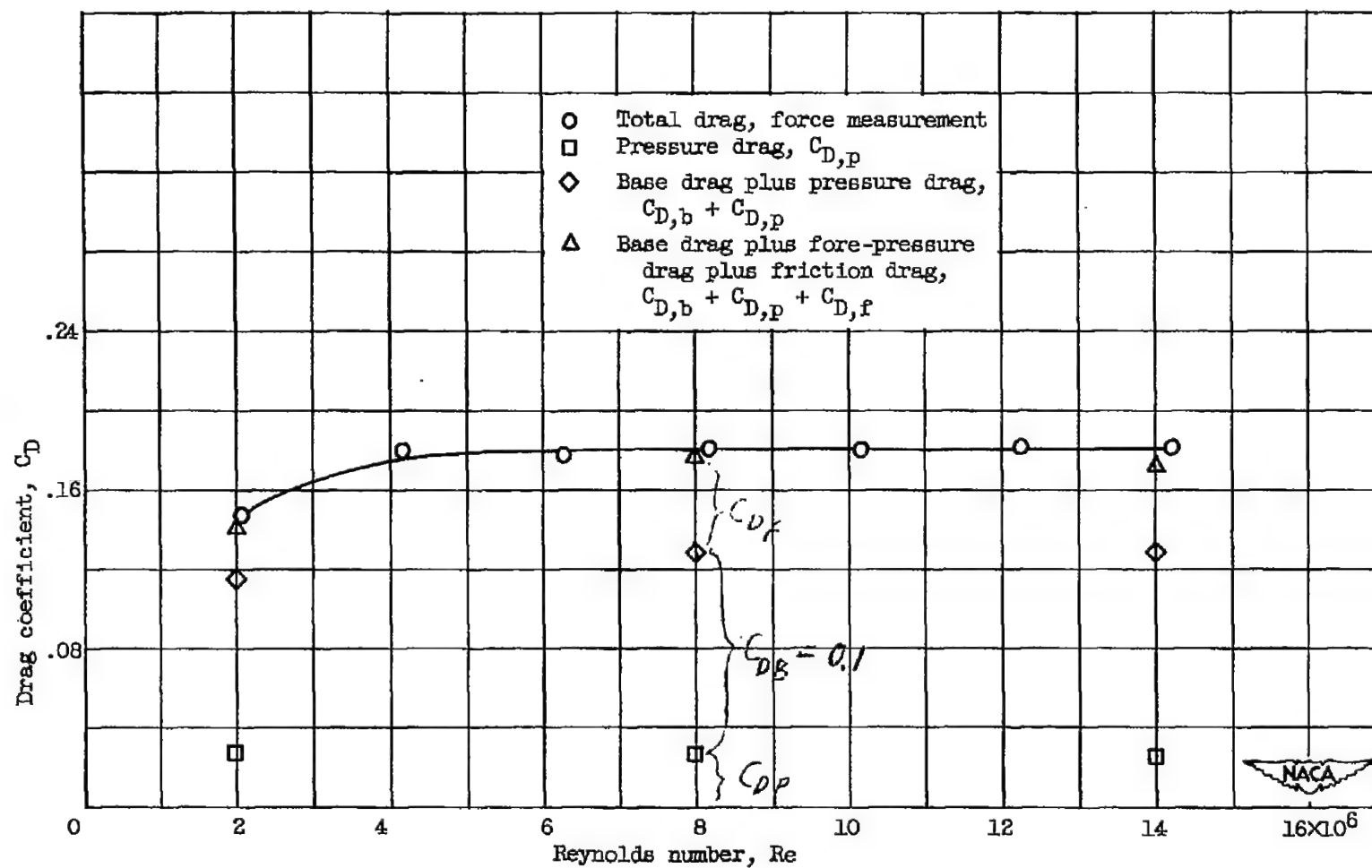
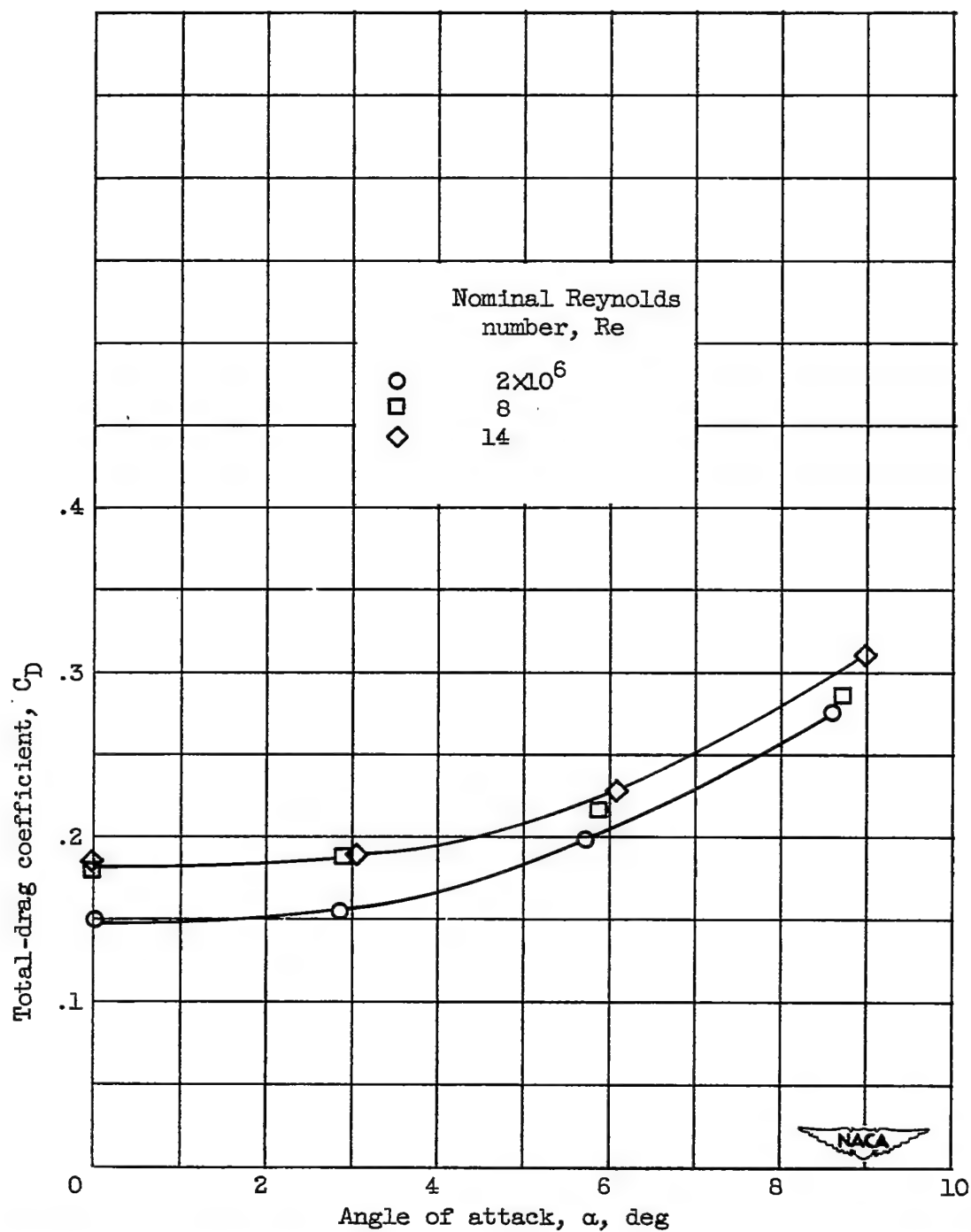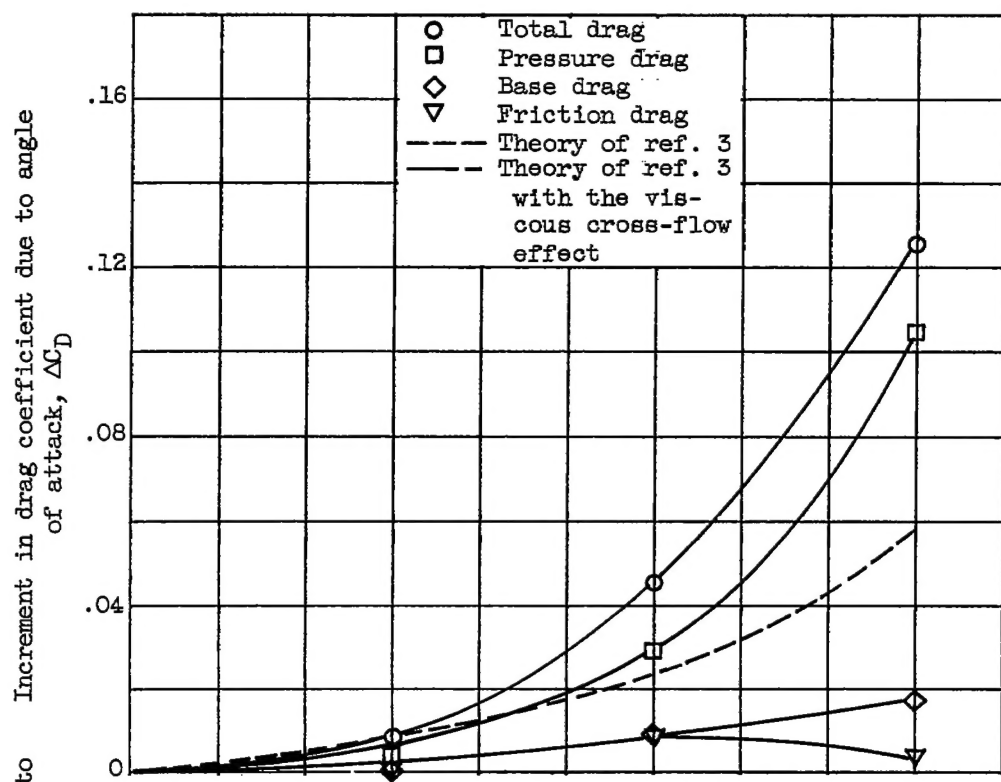Figure 8. - Variation of drag coefficient with free-stream Reynolds number for zero angle of attack.
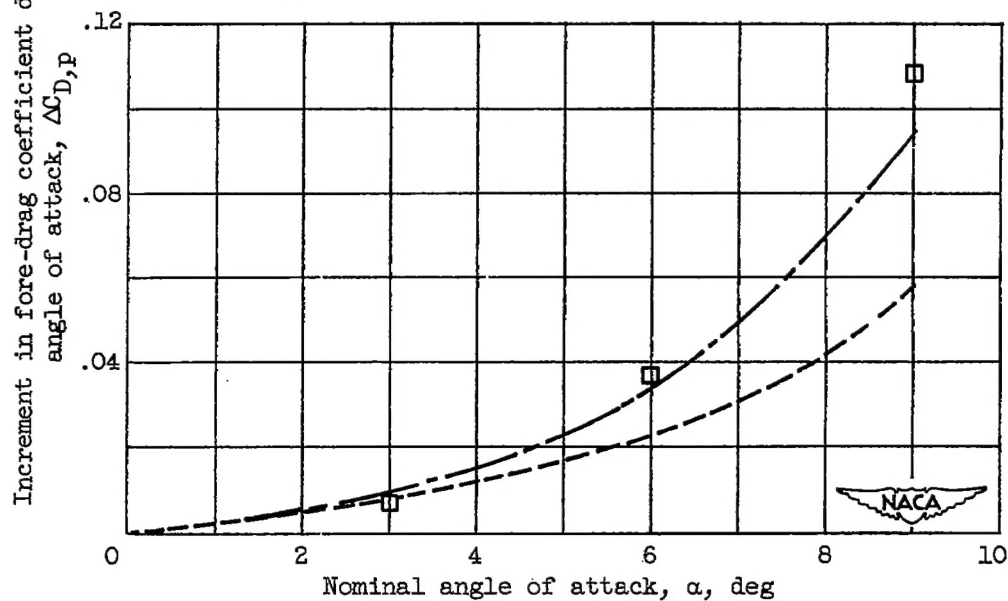
2738

Figure 9. - Variation of total-drag coefficient with angle of attack
for three Reynolds numbers.

Legend:
- ○ Total drag
- □ Pressure drag
- ◇ Base drag
- ▽ Friction drag
- — — — Theory of ref. 3
- — · — Theory of ref. 3 with the viscous cross-flow effect

(a) Increment in total-drag components.

(b) Increment in fore-drag.

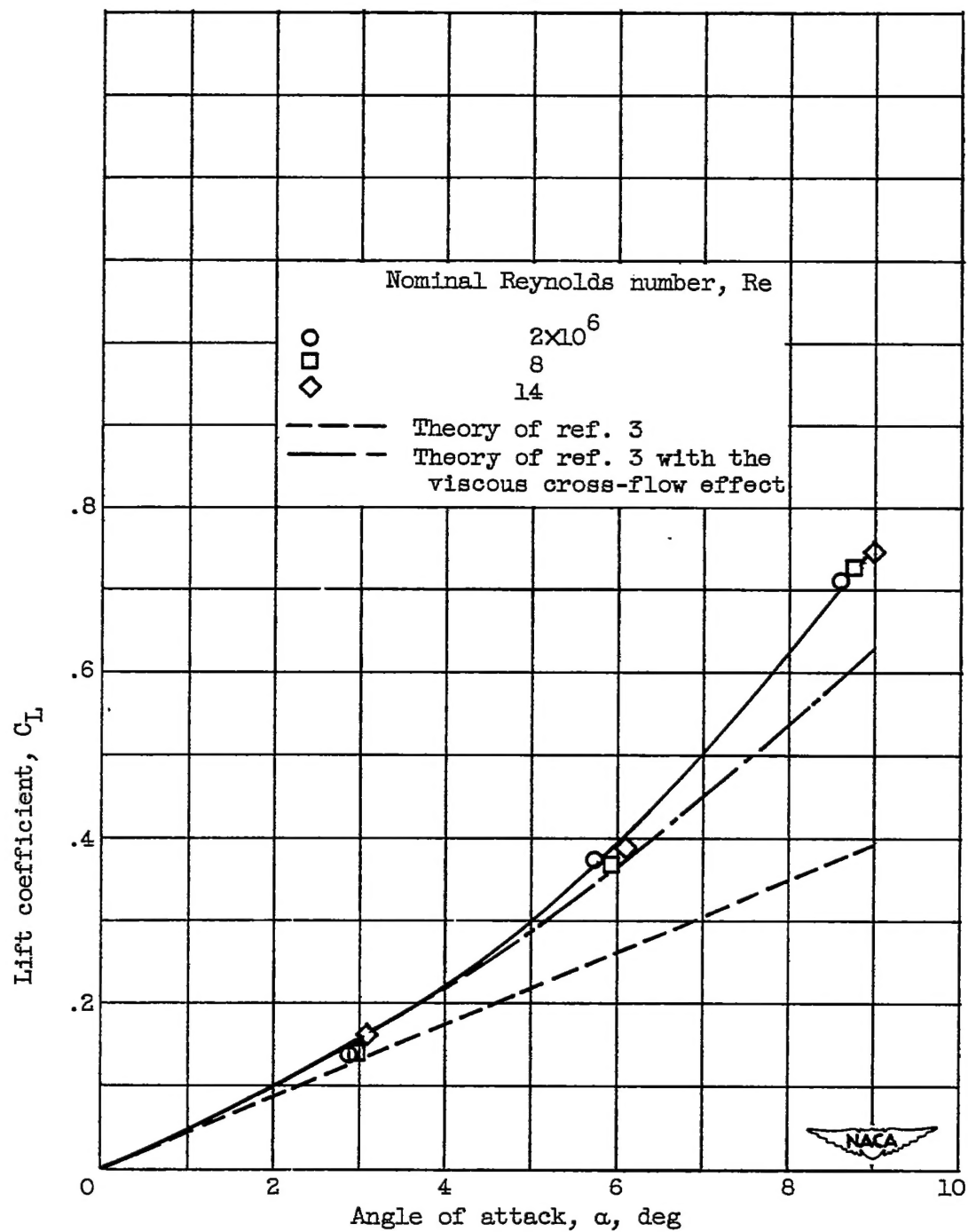Figure 10. - Increment in drag coefficient due to angle of attack for Reynolds number of 14×10^6.

2738

Figure 11. - Variation of lift coefficient with angle of attack for three Reynolds numbers.
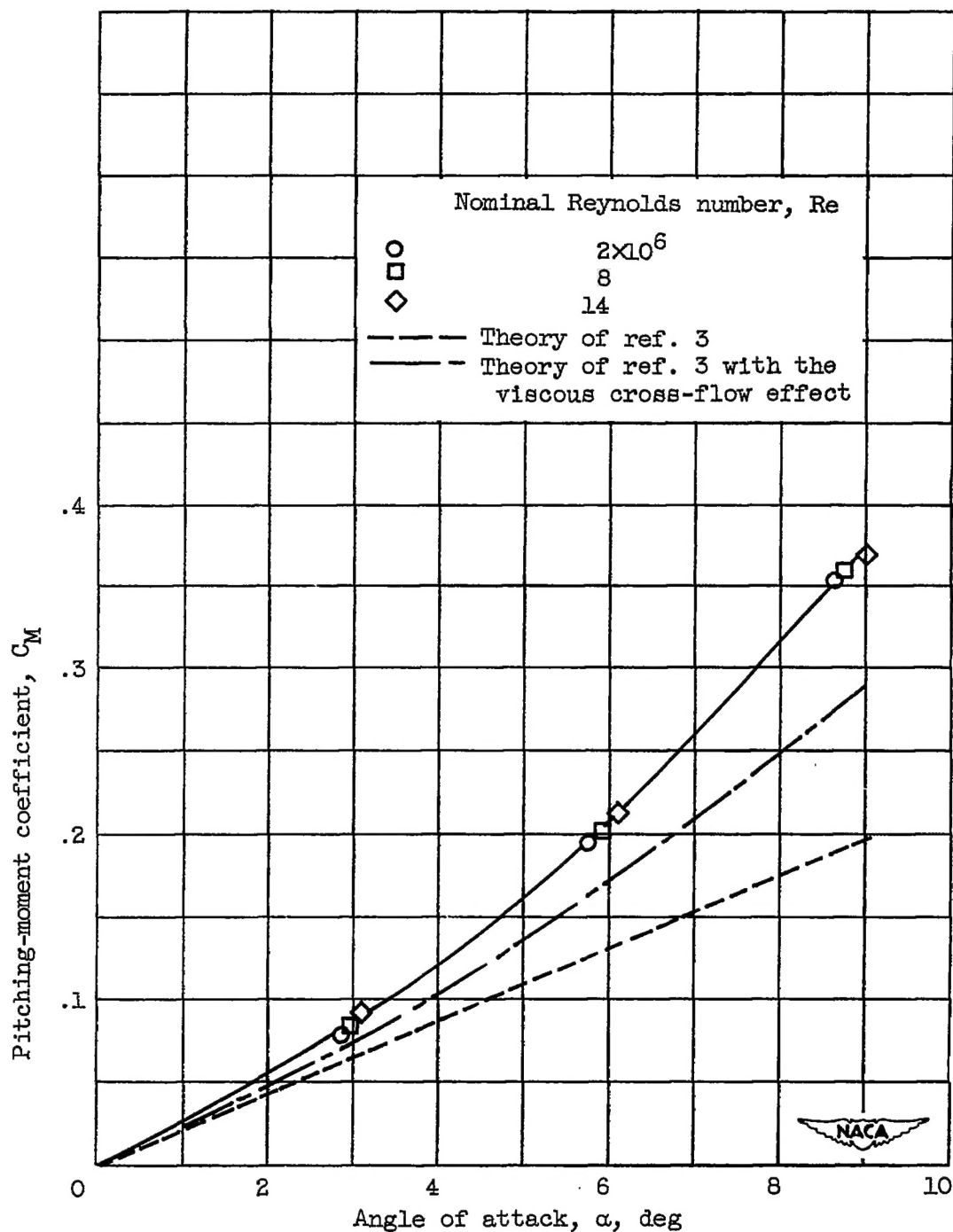
Figure 12. - Variation of pitching-moment coefficient with angle of attack for three Reynolds numbers.
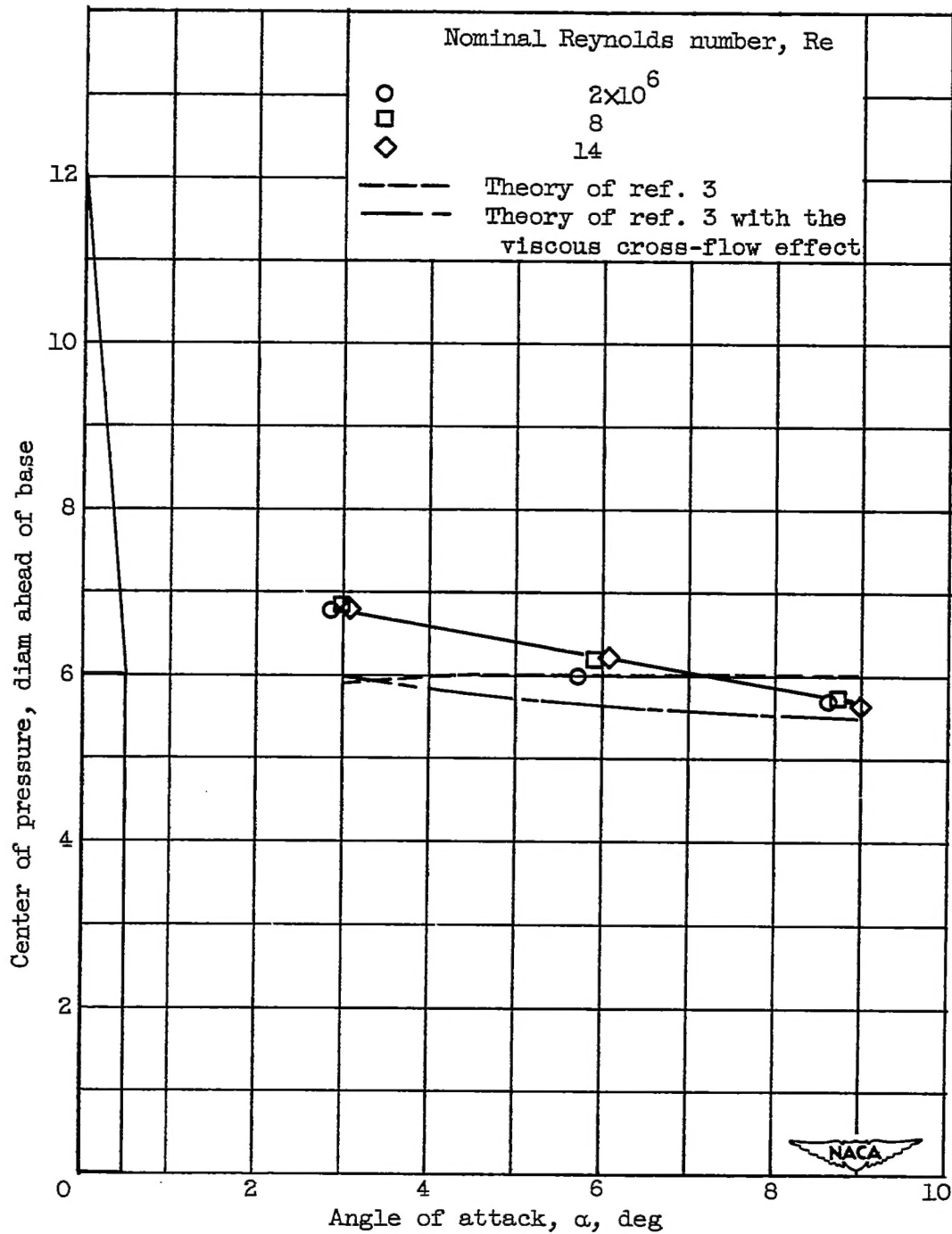
Figure 13. - Variation of center of pressure with angle of attack for three Reynolds numbers.